Test and Analysis Correlation for Sandwich Composite Longitudinal Joint Specimens

Brian H. Mason*, Arunkumar Satyanarayana†, and David W. Sleight‡
NASA Langley Research Center, Hampton, VA, 23681-2199

The NASA Composite Technology for Exploration (CTE) project is tasked with evaluating methods to analyze and manufacture composite joints for potential use in block upgrades to the Space Launch System (SLS) launch-vehicle structures such as the Payload Attach Fitting (PAF). To perform this task, the CTE project has initiated test and analysis correlation studies for composite joints under various loading conditions. Herein, NASA-developed numerical models are correlated with the experimental results from a series of tension tests. Pretest strain results matched the far-field test data well, but did not capture the nonlinear response in the vicinity of the joint. A refined pretest analytical model was modified to represent progressive failure of the specimens at failure locations observed during the experimental tests. The nonlinear strain response from this progressive failure model predicted the delamination failure load within 15% of the test data, but underpredicted the nonlinearity of the strain response. Further study of composite material models that account for the nonlinear shear response of fabric composites is recommended for the composite joint structures considered in this paper.

I. Introduction

NASA is currently developing the next generation of launch-vehicles to perform crewed Mars missions and other interplanetary missions. A crucial component of the Space Launch System (SLS) vehicle used in these missions is the use of advanced materials in various structural components [1]. The SLS vehicle will be assembled from several stages. As shown in Fig. 1, the Universal Stage Adapter (USA) and Payload Attach Fitting (PAF) are connected to the Exploration Upper Stage (EUS) at a circumferential joint. The payload for the SLS is mounted atop the PAF. The diameter of the conical PAF is over 8 meters, which is too large to manufacture as one piece in all but the largest autoclaves; therefore, the PAF is being designed to be manufactured in eight sections connected with longitudinal joints.

The NASA Composite Technology for Exploration (CTE) project is tasked with maturing advanced composite technologies that may lead to new approaches for future launch vehicles (such as SLS) and transfer of these technologies to other government and industrial entities. The CTE project builds upon composite design and manufacturing knowledge obtained from earlier NASA programs [2 to 4]. Results from the CTE project may be used to develop future block upgrades to launch-vehicle structural components.

As an approach to advancing composite technologies, the CTE project is currently focused on the development of composite joints for a conical structure such as the SLS PAF due to its challenging joint geometries and loads compared to a cylindrical jointed structure. As part of this focus, composite joints for a generic PAF called the *CTE point design* are being designed with a goal of advancing the state of the art in the detailed analyses of composite bonded joints. The current state of the art analysis techniques for composite failure analysis include cohesive zone modeling (CZM) [5], the virtual crack closure technique (VCCT) [6-8], and progressive failure analysis (PFA) [9]. To help assess the structural performance of the CTE-point-design structure and validate the structural models for joint failure prediction, test and analysis correlation studies for composite joints under various loading conditions were conducted. In the CTE project, jointed test specimens to represent the structure under different loading conditions including axial compression, and circumferential tension, were manufactured. In this paper CZM tools were used to

*Research Aerospace Engineer, Structural Mechanics and Concepts Branch, NASA Langley Research Center, Mail Stop 190, Senior Member AIAA
†Aerospace Engineer, Structural and Thermal Systems Branch, NASA Langley Research Center, Mail Stop 431, Senior Member AIAA
‡Aerospace Engineer, Structural and Thermal Systems Branch, NASA Langley Research Center, Mail Stop 431, Senior Member AIAA

correlate with experimental results of the jointed specimens. Deficiencies in the predictive capabilities of current analysis methods are also documented in this paper. VCCT was not used due to project time constraints.

In this paper, the testing and analysis correlation of coupon specimens representing a longitudinal joint subjected to circumferential tension are described. As such, structural analysis models of the longitudinal joint specimens will be correlated with the failure modes and displacement and strain responses observed during the test. These specimens were cut from flat sandwich panels; therefore, although there is no panel curvature, the loading direction is referred to as circumferential tension in this paper.

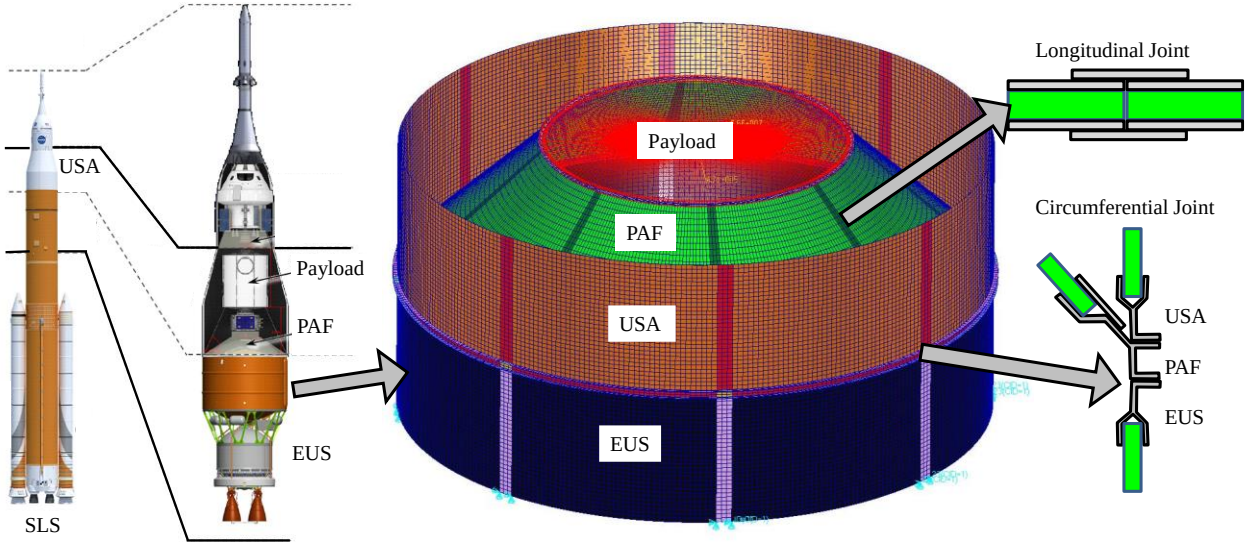

Figure 1. Exploded view of PAF and joints.

This paper is organized as follows. Section II contains a description of the longitudinal joint test specimen and the test setup. In Section III, four numerical models used for predictions of strains and failure loads are presented. Correlation of strains, displacements, and failure loads between the analytical models and experimental test data is discussed in Section IV. A summary of the approach used in the paper and the results of the study are presented in Section V.

II. Test-Article Geometry and Loads

In this section, the design and analysis details for the longitudinal composite bonded joint in tension is described. The parent panel from which the test specimens were cut is described first. Next, the model geometry and the configuration for the experimental tests are described. Experimental testing was conducted at Southern Research in July 2018 in Birmingham, AL. In the third part of this section, the finite element (FE) model that simulates the longitudinal joint is discussed.

A. Parent Bonded Joint Test Panel

The parent material for the considered test articles was from two jointed panels manufactured specifically for the CTE project at the NASA Marshall Space Flight Center (MSFC). The panels were of sandwich construction with 3.1-lb/ft^3, 1-in. thick perforated Hexcel[§] aluminum core (5056) with (3/16-in.) hexagonal cells and 8-ply quasi-isotropic carbon fiber/epoxy face sheets with a layup of $[45/90/-45/0]_S$. The face sheets were constructed with Hexcel IM7/8552-1 prepreg slit-tape. The adhesive used to join the face sheets to the core was FM209-1M where the "M" after each designation refers to random glass mat finish. The panel was laminated on a flat composite tool using an automated tape laying process with ½-in.-wide unidirectional preimpregnated slit tape. Both face sheets and the core were cured in a single autoclave cycle. In a secondary bonding process, doubler plates were bonded to the sandwich panels to form the investigated joint. The material for the doubler plates was T650/5320-1 epoxy and carbon fiber

[§] The use of trademarks or names of manufacturers in this report is for accurate reporting and does not constitute an official endorsement, either expressed or implied, of such products or manufacturers by the National Aeronautics and Space Administration.

woven prepreg doubler plates with a layup of $[45]_4$. Doubler plates were bonded to the sandwich panels with FM209-1M adhesive. The doubler plates were 4.2-in. long with 0.9-in. of taper at both ends (as shown in Fig. 2). During the joining process, an adhesive paste (EA 9396 6MD) was injected to fill a 0.1-in. gap between the two panel segments. After this bonding process, the joined panel was sectioned into circumferential tension coupon test specimens. The width of these specimens was 3-in. The schematic of the bonded joint is shown in Fig. 2. In Fig. 3, one of the two parent bonded joint panels is shown, prior to cutting into circumferential tension specimens.

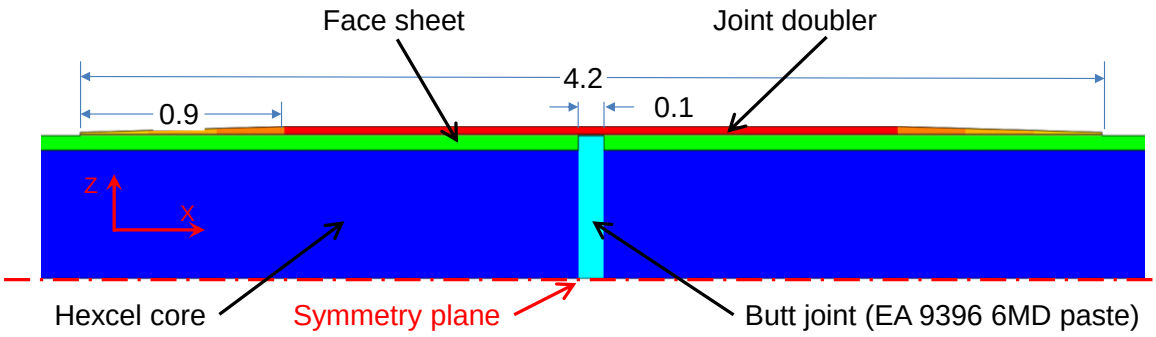

Figure 2. Bonded joint details (all dimensions in inches).

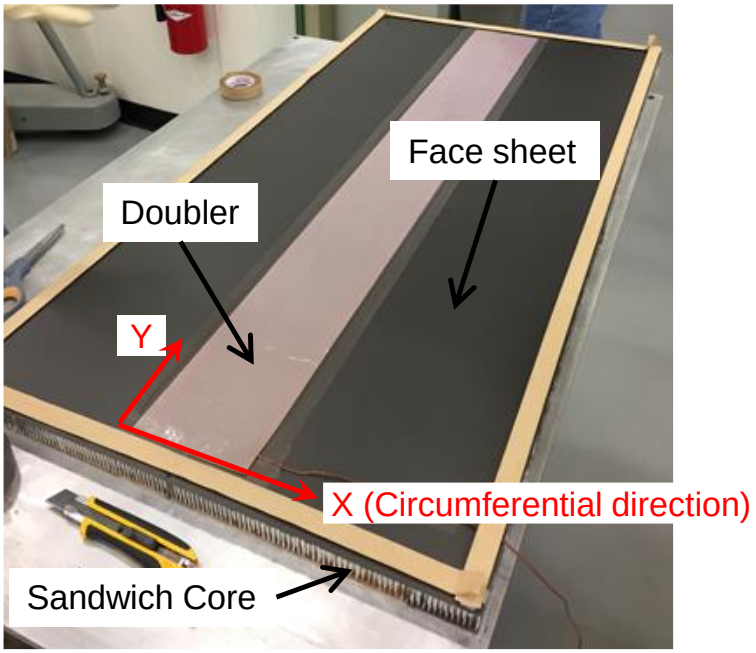

Figure 3. Jointed composite sandwich panel, prior to cutting into test specimens.

B. Experimental Test Configuration

The two bonded-joint composite sandwich panels were machined into test specimens with dimensions of 22 in. by 3 in. The test specimens are designed to fail at the joint location, and will be discussed in Section III. Later some of the test specimens were impacted to produce local damage. In all, ten pristine and nine impact-damage specimens were tested. Only results for the pristine specimens are presented in this paper.

The maximum space between the grip faces in the chosen test machine was 0.6 in.; hence, the circumferential tension test specimen was designed to fit within the grips by using tapered inserts at each end. The core at the load introduction ends of the specimens was removed to a depth of 3.4 in. and an aluminum insert which was 1 in. thick at the core and tapered to 0.6 in. at the free end was inserted at either end of the panel and attached to the face sheet with adhesive (See Fig. 4). The surface of the aluminum insert was prepared using the Cytec BR 127 corrosion inhibiting primer, and the face sheet was prepared with hand abrasion followed by solvent wipe before the aluminum insert was bonded to the specimen using Henkel Loctite Hysol EA 9394 epoxy adhesive cured at room temperature.

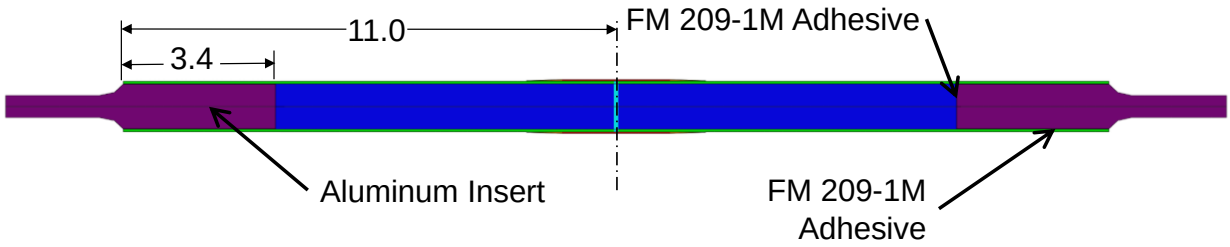

Figure 4. Test specimen dimensions (all dimensions in inches).

Instrumentation included conventional strain gages, a high-speed digital camera to capture the failure sequence at the joint, and one 2D digital image correlation (DIC) system. A speckle pattern was optimized for a measurement area of 3-in. wide by 22-in. long and covered one entire side of the test article for full-field displacement and strain measurements with DIC. The DIC systems were monitored in real time and data was saved at the rate of one frame per second.

Five of the ten tension coupon were instrumented with a total of ten strain gages. The location of the gages are shown as red and yellow circles (and labeled as SG 1 to 10) in Fig. 5. The remaining five specimens were instrumented with only two strain gages (SG1 and 2). The six strain gages shown in red in Fig. 5 were installed on the side without the DIC speckle pattern, in order to avoid interference with the DIC measurements. The two yellow circles in Fig. 5 represents back-to-back strain gages (four total), which are used to determine the bending response of the specimen and for initial alignment of the specimen. For test-analysis correlation, displacements were computed from DIC data between points labeled D1 and D2 in Fig. 5. The actual test setup is shown in Fig. 6. Resolution of the DIC data is 0.125 in. with a displacement accuracy of 0.14 mils.

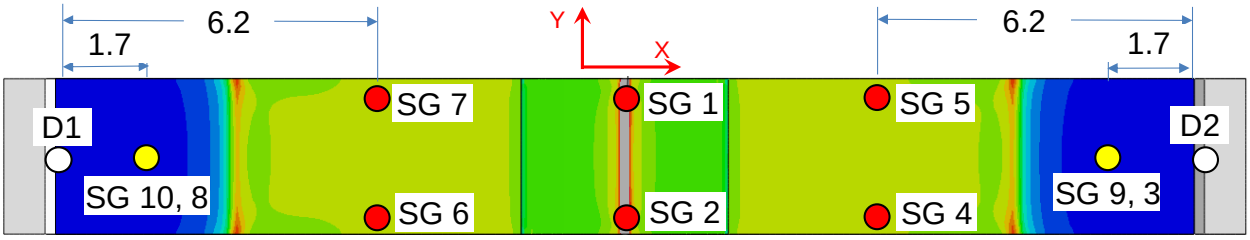

Figure 5. Strain gage locations (all dimensions in inches).

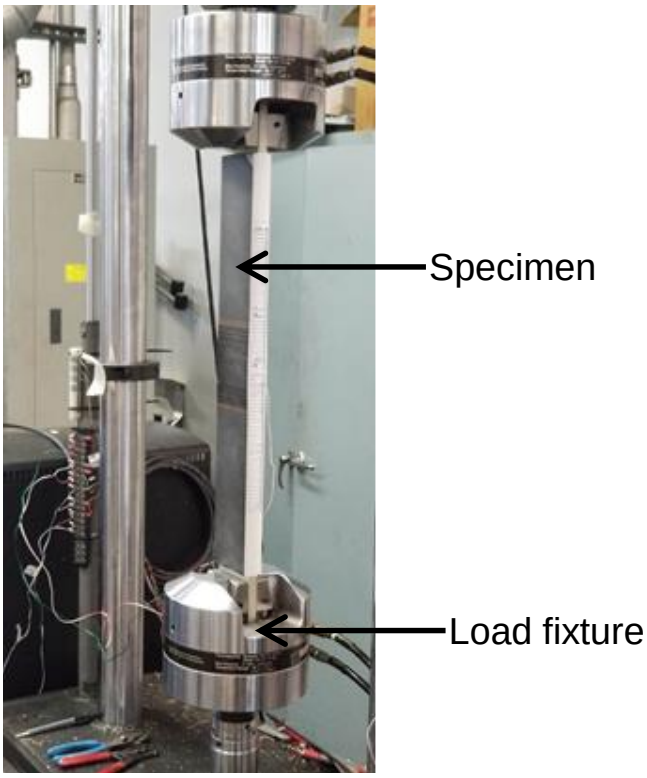

Figure 6. Test configuration.

During manufacturing of the specimens from the first panel (identified as panel CTE-300-3), nonconformities in the alignment of the aluminum inserts was observed with all five specimens cut from this panel. The nonconformities include both misalignment of the inserts with respect to each other and misalignment with respect to parallelism of the inserts with respect to the specimen, as shown in Figure 7. The amount of nonconformity for each specimen is presented in Table 1. Specimens manufactured from the second panel (CTE-300-1) were within tolerance (0.002 in.). All ten specimens were tested at Southern Research in July 2018. While these specimens are out of tolerance, they were still used successfully in the test program.

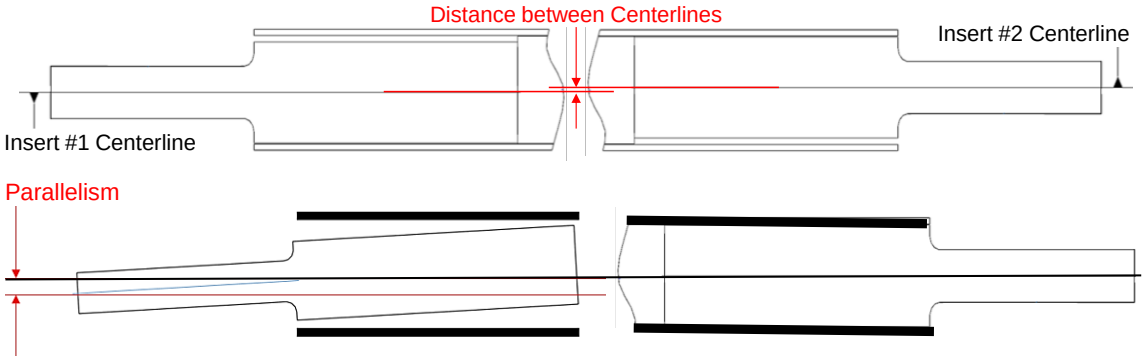

Figure 7. Alignment nonconformities.

Table 1. Alignment nonconformities for five specimens.

Measurement of Misalignment	CTE-300-3-HT-P-1	CTE-300-3-HT-P-2	CTE-300-3-HT-P-3	CTE-300-3-HT-P-4	CTE-300-3-HT-P-5
Distance between centerline of inserts 1 and 2, in.	0.0187	0.2456	0.1384	0.0924	0.1158
Parallelism of insert 1 with respect to insert 2, in.	0.0012	0.0173	0.0163	0.0083	0.0094

III. Numerical Models

In general, a bonded joint can fail due to debond/delamination between face sheet plies and doubler plies, as well as fiber and matrix damages either in face sheets or joint doubler plates. Also, there could be damages in the core, the core/face sheet adhesive layer, the face sheet/doubler adhesive layer, and the gap filler material which all lead to catastrophic failure of the joint. Simulation of all the above defined damage modes can be accomplished through various damage models. In this section, four finite element (FE) models are discussed. The first model was a coarse linear static model using an in-plane failure criterion. Models 2 and 3 had a more refined-mesh than Model 1 and were created as part of a mesh convergence study. Additionally, a nonlinear analysis was performed with Model 3 using plasticity to simulate failure in the gap filler material. The last model was a modified version of Model 3, which includes delamination using a cohesive zone model (CZM).

A. Coarse Model

For pretest prediction, a relatively coarse FE model was created and used only strength-based first ply failure criterion to predict a failure load. Analyses were performed using the general-purpose FE code Abaqus [10]. An initial FE model, Model 1, consisting of 72,880 elements and 92,496 nodes, is shown in Fig. 8. Model 1 consisted of 8-node solid hexahedral continuum elements (C3D8) for the sandwich core and aluminum inserts, and 8-node continuum shell elements (SC8R) for the adhesive, face sheets, and doubler plate. This model was symmetric about the middle of the core section, as illustrated in Fig. 6. A quarter-symmetry model was not used; because, the ply angles would be incorrectly reversed across the symmetry plane. The element discretization in this model was relatively coarse, with a far-field element length of 0.10 in. and a length of 0.05 in. in the vicinity of the doubler plate. The elements were 0.075 in. wide. In this initial model, the doubler plate was attached to the face sheet with multi-point constraints (MPC) at coincident nodes.

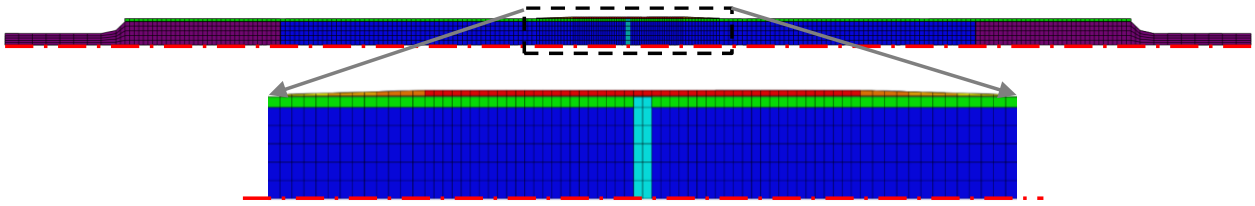

Figure 8. Model 1.

Material properties used in this study were obtained from CTE equivalency tests, which are not referenceable. However, the material properties were similar to room temperature lamina data from the National Center for Advanced Material Performance (NCAMP) provided in Table 2 [12, 13]. All strength properties in Table 2 were mean values, not B-basis. Material properties for the gap filler are similar to those presented in Table 3 [14].

Table 2. Material properties for carbon fiber lamina.

Property	IM7/8552-1 [12] Face sheets	T650/5320-1 [13] Doubler plates
Nominal Ply Thickness, in.	0.0072	0.0077
Elastic Modulus – Longitudinal, Msi	20.44	9.37
Elastic Modulus – Transverse, Msi	1.30	8.88
Shear Modulus, Msi	0.68	0.74
Poisson's Ratio	0.356	0.053
Tensile Strength – Longitudinal, ksi	371.1	124.9
Tensile Strength – Transverse, ksi	9.3	121.8
Compressive Strength – Longitudinal, ksi	-251.1	-106.2
Compressive Strength – Transverse, ksi	-41.4	-100.4
Shear Strength, ksi	13.2	14.7

Table 3. Material properties for gap filler.

Property	EA9396.6 MD gap filler [14]
Elastic Modulus, ksi	400
Tensile Strength, ksi	8.0

A linear static analysis of Model 1 was conducted in Abaqus using an applied end displacement of 0.0886 in. The corresponding load for this applied displacement is 14.43 kips (14,430 lbf). The Tsai-Hill first ply failure index, in which a value of unity indicates failure, was used to evaluate the strength of this model [11]. This displacement was determined by interpolation to produce a maximum Tsai-Hill failure value of 1.0 in the model. Contours for the Tsai-Hill failure index are presented in Fig. 9 and indicate that in-plane failure is likely to initiate at the joint (as desired) instead of in the load application region.

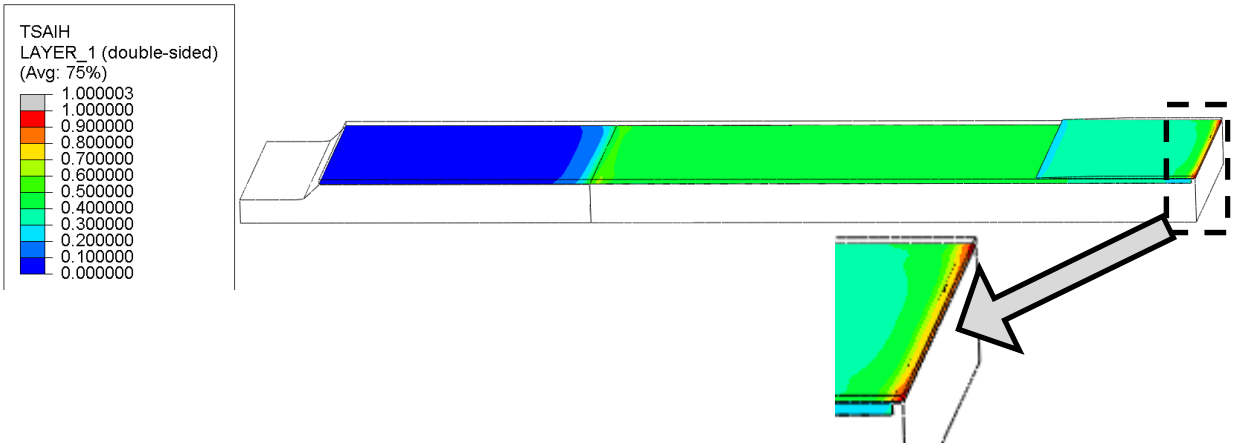

Figure 9. Tsai-Hill failure index at doubler failure load of 14.43 kips (half model) in Model 1.

B. Intermediate Model

A second model of the tension specimen with an increased mesh discretization was created to evaluate the effect of mesh refinement on the results. The intermediate model, Model 2, consisting of 942,500 elements and 1,012,424 nodes, is shown in Fig. 10. The element discretization was increased over Model 1, with an element length of 0.033 in. in the vicinity of the doubler plate and an element width of 0.03 in.

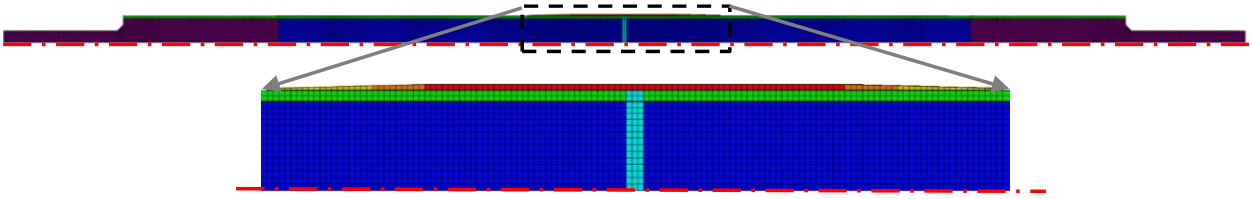

Figure 10. Model 2.

A linear static analysis of Model 2 was conducted in Abaqus using the same applied end displacement used in Model 1 (0.0886 in.). The corresponding load for this displacement is 14.19 kips which is within 2% of the load in Model 2. Contours for the Tsai-Hill first-ply failure index for Model 1 and 2 are similar, but the maximum Tsai-Hill value is 1.062; so, the local stresses around the joint are not considered to be converged.

C. Refined Model

A third model of the tension specimen with an increased mesh discretization was created in an attempt to improve the mesh convergence over Models 1 and 2. The refined model, Model 3, consisting of 1,429,650 elements and 1,784,820 nodes, is shown in Fig. 11. The element discretization was increased over previous models, with an element length of 0.02 in. in the vicinity of the doubler plate and an element width of 0.02 in.

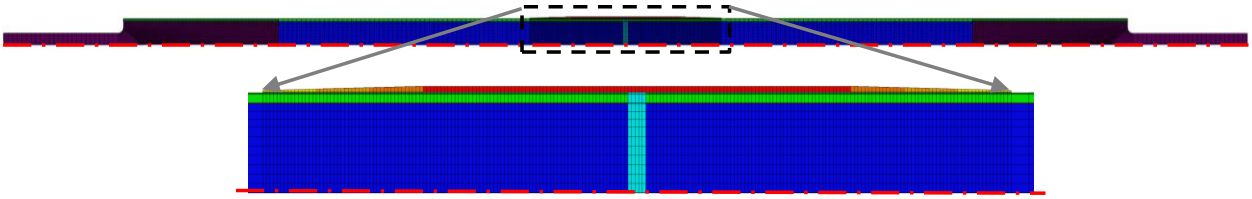

Figure 11. Model 3.

Two analyses were conducted with Model 3. First, a linear static analysis was conducted in Abaqus using an applied end displacement of 0.0886 in. The corresponding load for this applied displacement is 14.33 kips, which is within 1% of the load for both Models 1 and 2. Contours for the Tsai-Hill first-ply failure index for Model 1 and 2 are similar, but the maximum Tsai-Hill value is 1.095. Based on the failure index, the stresses in Model 3 are 3% higher than Model 2; so, the mesh refinement is considered to be converged.

A geometrically nonlinear static analysis of Model 3 was conducted, but the stress results differed from the linear analysis by less than 2%; so these results are not reported in this paper. Instead, another nonlinear implicit static analysis was conducted which also included a plasticity model for the gap filler material. Because the strength of the gap filler is less than the strength of the composite materials, it is expected that the gap filler will fail at a lower load than the rest of the structure. As a simplified method of simulating failure in the gap filler, a plasticity model was used for the gap filler in which the gap filler reacts as a purely plastic material at loads above yield strength. The material properties used for the gap filler material are shown in Fig. 12. In Fig. 12, the stresses are normalized by the failure stress of the material.

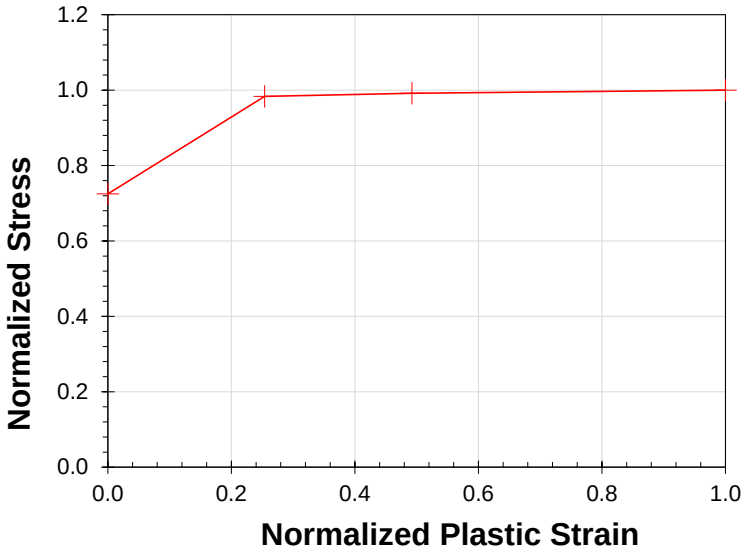

Figure 12. Stress vs. plastic strain of gap filler.

Contours for the Tsai-Hill failure index from the nonlinear plasticity analysis of Model 3 are presented in Fig. 13. The Tsai-Hill value in the face sheet and the doubler plate are 0.707 and 1.599, respectively; so, failure is predicted to initiate at the doubler plate. The Tsai Hill value is 46% higher than in the linear analysis for Model 3 due mostly to nonlinearity in the gap filler. The deformations of Model 3 from both a linear and nonlinear plasticity analysis are shown with magnification factor of 20 in Fig. 14. In the joint region, the tension load is carried by the doubler plate instead of the face sheets, and this load eccentricity causes localized bending at the joint. The localized bending effect is much larger in the plasticity model than in the linear model.

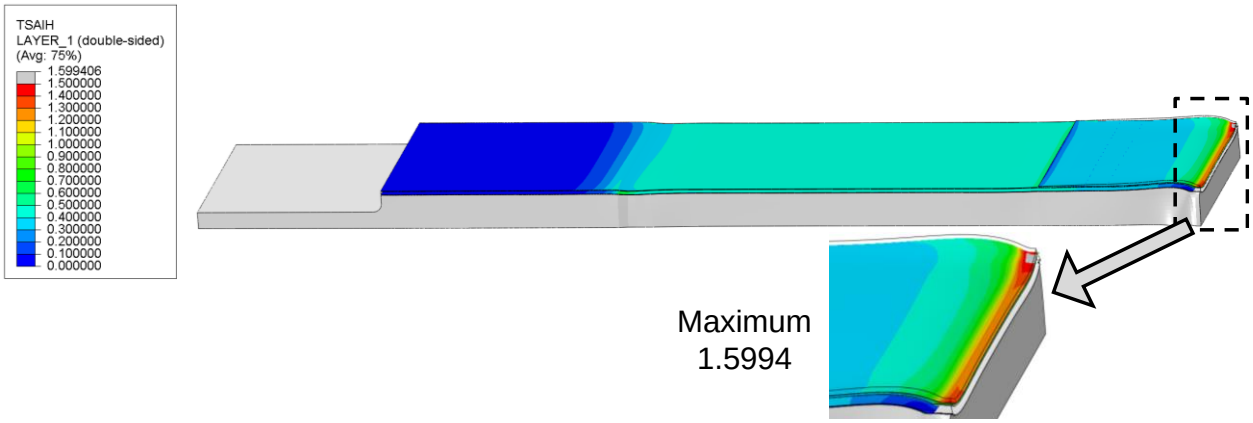

Figure 13. Tsai-Hill failure index at 14.33 kip load (half model) in Model 3 (nonlinear analysis).

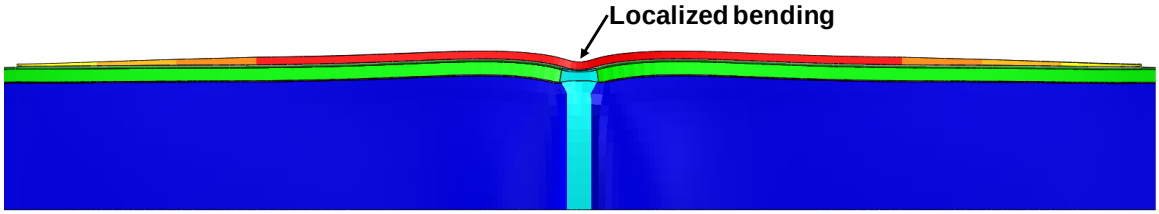

a) Model 3, Linear (No Plasticity)

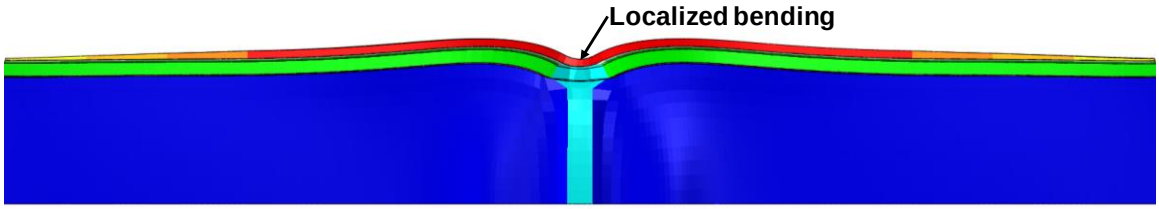

b) Model 3, Nonlinear (with Plasticity in Gap Filler)

Figure 14. Deformed shape of Model 3 without and with gap filler plasticity (deformations magnified by 20).

D. Delamination Model

Due to the loading configuration for this tension specimen, the interlaminar stress in the face sheet plies and/or doubler plies were expected to dominate the failure process in the form of delamination. Hence, Model 4 of the specimen was created from the mesh of Model 3 by replacing MPCs in the vicinity of the joint with a cohesive layer between face sheet plies. To simulate delamination between the ply interfaces, the cohesive zone model (CZM) available in Abaqus software was employed along with an explicit dynamic analysis procedure. Fracture toughness parameters for the IM7/8552 tape interface used in the CZM were obtained from Ref. 12, and other parameters were computed using the equations in Ref. 5, as presented in Table 4.

Table 4. Interface properties for IM7/8552.

Property	Tape/Tape Interface
Mode I Interlaminar Fracture Toughness (G_{Ic}), lbf/in.	1.37 [12]
Mode II Interlaminar Fracture Toughness (G_{IIc}), lbf/in.	4.22 [12]
Mode I Penalty Stiffness (K_I), Msi	1300.0 [5]
Shear Penalty Stiffness (K_{sh}), Msi	630.0 [5]
Maximum Nominal Normal Stress(U_I), ksi	5.141 [5]
Maximum Nominal Shear Stress (U_{II}), ksi	12.644 [5]

Another possible failure mode for the joint is in-plane (fiber and matrix) damage in the doubler plate. The Abaqus software does include an in-plane damage model that uses failure criteria such as Hashin-Rotem [15], but accurate failure data for the fabric doubler were not available for input to this failure procedure. For in-plane net-section failure of the doubler plate, the Tsai-Hill first ply failure criterion is the only failure analysis presented in this paper.

Out of plane deformation near the failure load (9.07 kips) are presented in Fig. 15. Fig. 15a shows the deformed state just prior to delamination. Fig. 15b shows the deformed state shortly after delamination. It can be noticed from Fig. 15 that delamination initiates in the joint region (between face sheet plies 7 and 8). Because failure analysis of the fabric doubler plates is not performed in this model, the crack path in the doubler plates is not simulated.

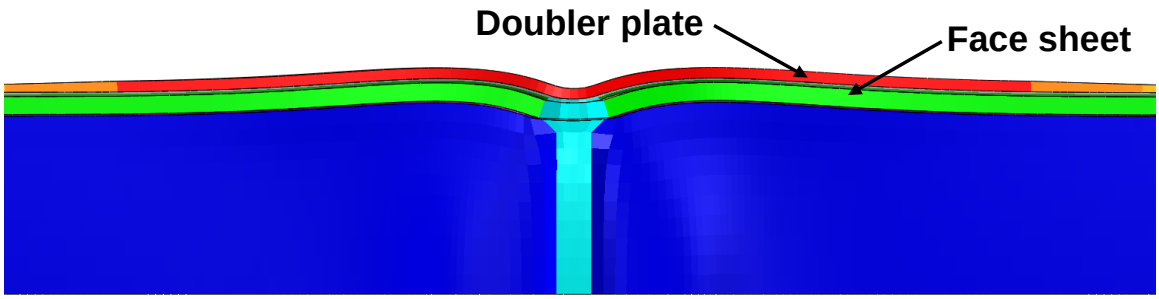

a) Model 4, 11.22 kip Load (Prior to Delamination)

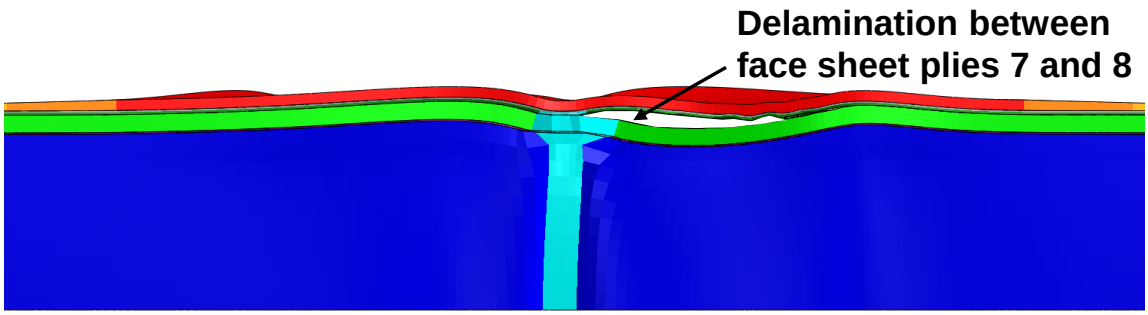

b) Model 4, 11.70 kip Load (After Initiation of Delamination)

Figure 15. Delamination in Model 4.

E. Comparison of Failure Load Predictions

Preliminary tension load predictions are based on analysis in Abaqus, which assumed nominal ply thicknesses and material properties. For evaluation of mesh convergence, the load due to an applied displacement of 0.0886 in. for the four numerical models is presented in Table 5. The load calculated as a reaction to the applied displacement in all four models agree within 2%.

The predicted failure loads from the four numerical models for these tension test coupons are shown in Table 5. Failure of the adhesive in the butt joint between the sandwich panels was not evaluated due to a lack of data for the adhesive/core interface strength and because failure of the bond between the sandwich panels was not expected to affect the overall strength of the joint since the majority of the load passes through the doubler plates. The failure loads for Models 1 to 3 are based on Tsai-Hill first ply failure. In Model 1, failure at the face sheet is predicted to occur at a much higher load than in the doubler plate. Due to localized stresses, the failure load decreases with increased mesh discretization, but the failure load of the intermediate model (Model 2) is within 3% of the failure load from the refined model (Model 3). A non-linear analysis with plasticity in the gap filler was performed with Model 3. The failure load in Model 3 with plasticity is 33% lower than with the linear elastic material; so, failure of the gap filler is likely to reduce the first ply failure load for the doubler plate.

The failure load for Model 4 is based on delamination of the top layer of the face sheet. Because in Model 4 delamination is considered without in-plane failure of the doubler plate, the predicted failure load for Model 4 is 33% higher than in Model 3 with plasticity.

Table 5. Predicted loads and reaction forces.

Model	Failure Location	Predicted Load at Failure (kip)	Load due to applied 0.0886 in. Displacement (kip)
1 (Coarse)	Face sheet at aluminum insert	21.74	14.43
	Doubler plate (Linear)	14.43	
2 (Intermediate)	Doubler plate (Linear)	13.36	14.19
3 (Refined)	Doubler plate (Linear)	13.13	14.33
	Doubler plate (Nonlinear)	**8.79**	14.06
4 (Delamination)	Face sheets (Nonlinear)	**11.70**	N/A

IV. Test-Analysis Correlation

This section includes the results for the CTE circumferential tension joint subelement tests conducted at Southern Research. Test results are compared with the numerical results from the three models that were discussed in section III. Five coupon specimens were cut from each of two panels (identified as panels CTE-300-1 and CTE-300-3) for a total of ten coupon specimens. Results such as end extension, strains at the joint, and failure load are presented. The dominant failure mode based on visual examination of each coupon are reported. Also, strain contour data from digital image correlation (DIC) system are discussed

A. Failure Loads and Modes

In Table 6, the failure loads, axial strain at center of the joint before failure, and failure modes of all 10 coupons are reported. The average failure load of the joint in tension, is 15.01 kips. The design limit load for this joint for the CTE project is 2.7 kip; so the average failure load is 5.56 times the design limit load. The failure modes of these coupons were delamination between face sheet plies, net section failure (NSF) of the doubler plates, and a "mixed" mode which means it was not apparent whether failure initiated with delamination or NSF. Pictures of three of the post-test coupons are shown in Fig. 16 to illustrate the three identified failure modes. Two of the coupons failed due to delamination of the outermost ply of the face sheet, adjacent to the doubler plate interface. Four of the coupons failed due to NSF of the doubler plates. In the remaining four coupons, it is not apparent if face sheet delamination or NSF of the doubler plate occurred first. However, the panels with delamination seemed to fail between loads of 13.0 kips and 13.9 kips, while doubler plates failed at higher loads ranging between 15.0 kips and 16.1 kips. It is also worth noting that in the coupons cut from panel CTE-300-3, the inserts were misaligned by up to 0.25 in. as was shown in Table 1; the specimens from this panel tended to fail due to NSF.

Table 6. Test data for pristine coupons.

Coupon ID	Test Failure Load (kips)	Strain at Failure in SG-1 (in./in.)	Failure Mode
CTE-300-1-HT-P-1	16.12	0.0200	Mixed
CTE-300-1-HT-P-2	13.77	0.0140	Mixed
CTE-300-1-HT-P-3	15.58	0.0197	Mixed
CTE-300-1-HT-P-4	13.00	0.0138	Delamination
CTE-300-1-HT-P-5	13.90	0.0150	Delamination
CTE-300-3-HT-P-1	15.67	0.0260	Net Section
CTE-300-3-HT-P-2	15.20	0.0270	Net Section
CTE-300-3-HT-P-3	15.02	0.0220	Mixed
CTE-300-3-HT-P-4	15.89	0.0350	Net Section
CTE-300-3-HT-P-5	16.00	0.0290	Net Section
Average	**15.01**		

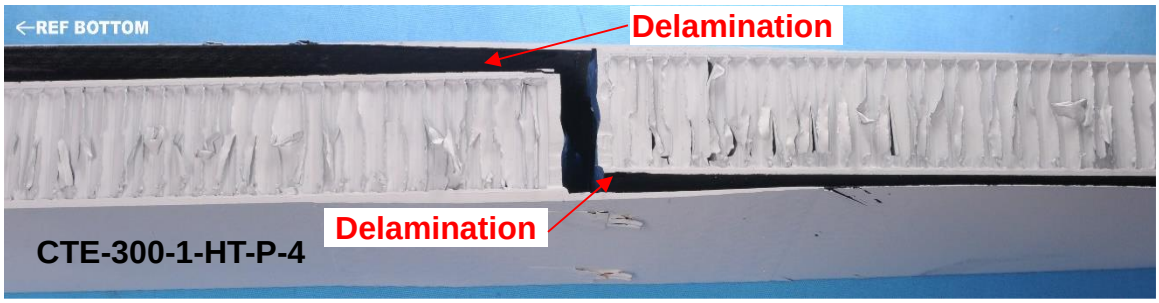

Delamination between face sheet plies

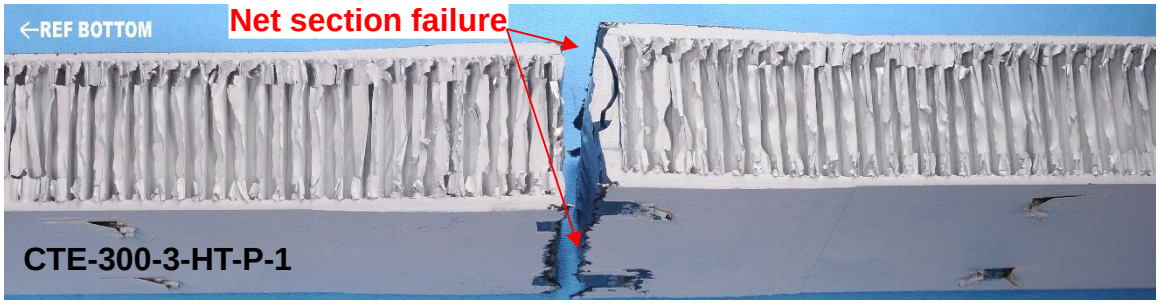

Net Section Failure

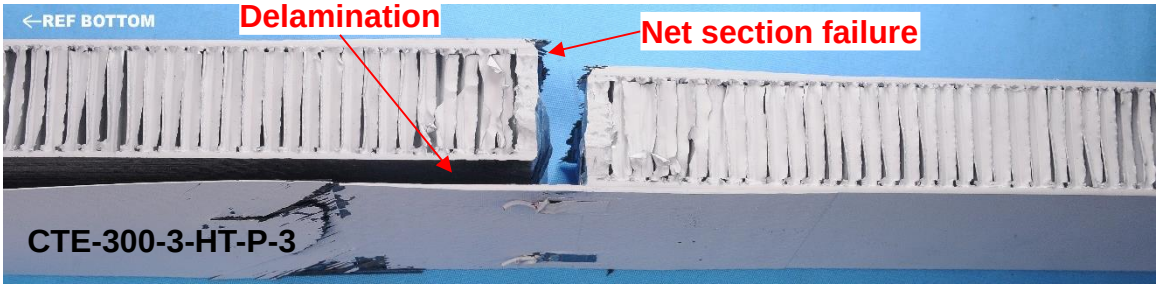

Mixed

Figure 16. Primary failure modes for tension specimens.

Load vs. end displacement data (measured between points D1 and D2 in Fig. 5) for two selected coupons are presented in Fig. 17. The two coupons were selected for the plot because DIC displacement data was available for the coupons and because they are representative and bracket the range of the failure loads. The slopes of the analysis data (stiffness) from linear analyses of Models 1 and 3 are within 0.03% of each other. The test data exhibit slightly nonlinear behavior above a load of 4 kips, and the slopes of the curves are about 6% and 3% lower than predicted by Models 1 and nonlinear Model 3, respectively. The predicted failure load for Model 3 is 45% below the failure load for the coupon 300-1-HT-P-1, which seemed to exhibit NSF. The slope of the analysis data from Model 4 is 3 to 4% below the slope of the test data, and the analysis data matches the slight nonlinearity of the test data well. The predicted failure load for Model 4 is 15% below the failure load for the coupon 300-1-HT-P-2, which seemed to exhibit delamination.

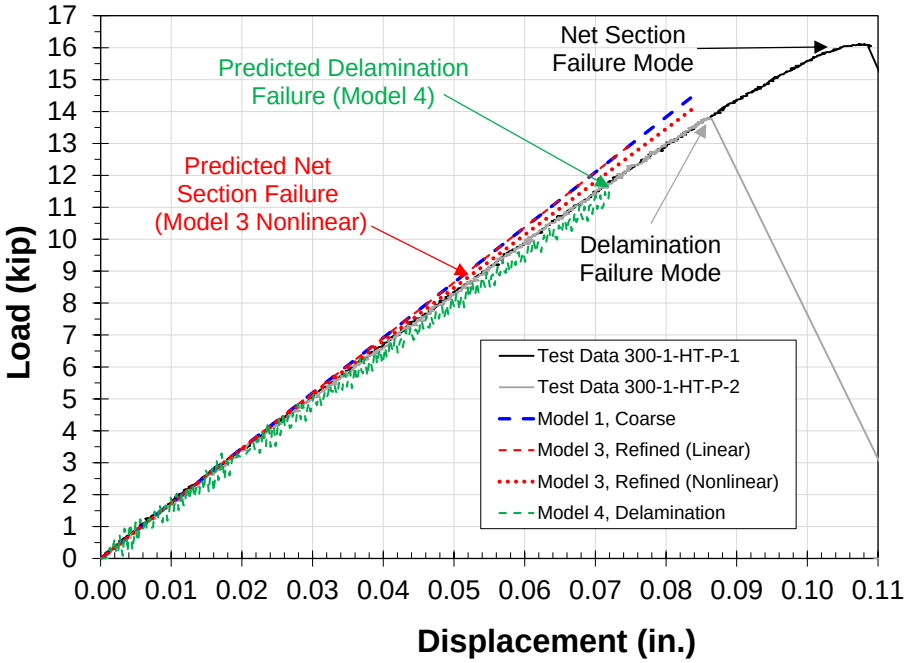

Figure 17. Load vs. end displacement.

B. Strain Data

Load vs. circumferential-direction strain data from strain gage 7 are presented in Fig. 18 and 19. Data from strain gage 7 represent a far-field strain gage 4.8 in. from the joint (see Fig. 5). Fig. 18 contains test data from five of the experimental tests, which agree well with each other. The test data are nearly linear until a load of 13 ksi. Fig. 19 contains test data from two representative specimens (300-1-HT-P-1 and 300-1-HT-P -2) and numerical data from Models 1 and 3. In Fig. 19, the predicted strain results from Models 1 and 2 are within 1% of the experimental strain values up to a load of 13 ksi, and slightly underpredict the stiffness response.

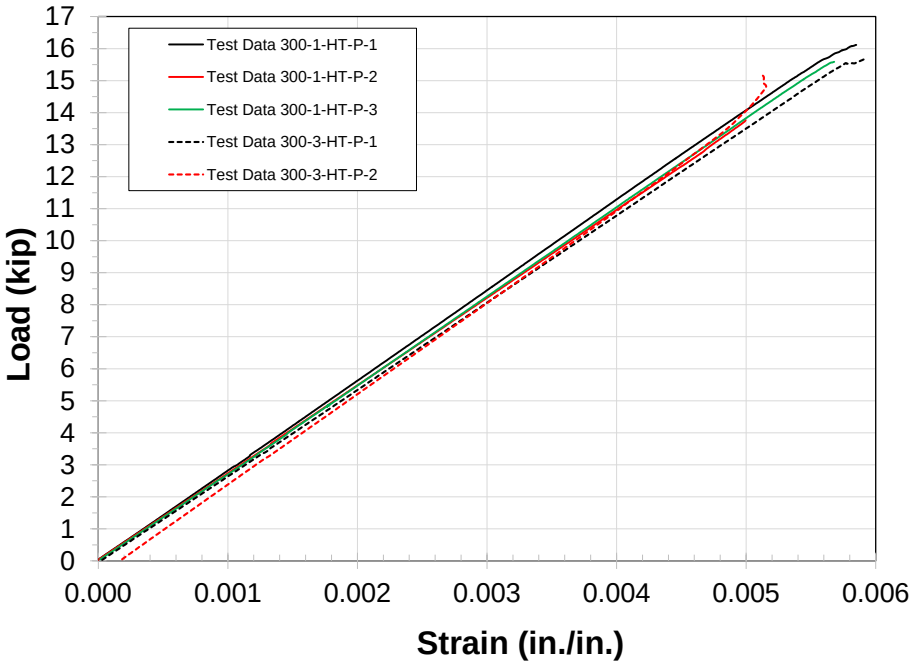

Figure 18: Load vs. strain test data for strain gage 7.

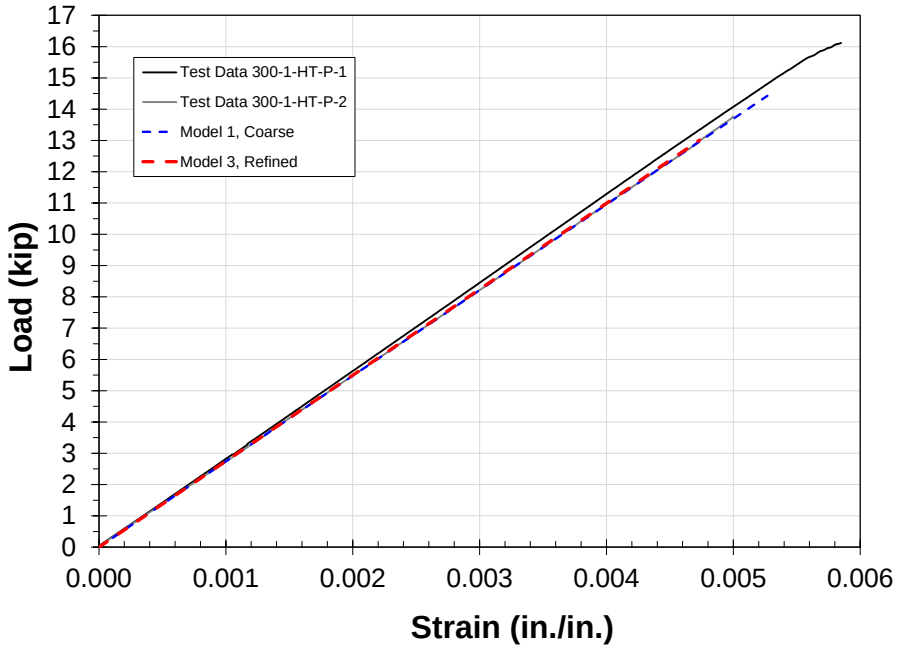

Figure 19: Load vs. strain test-analysis correlation for strain gage 7.

Load vs. circumferential-direction strain data from strain gage 1 are presented in Fig. 20. Strain gage 1 is in the joint region of the coupon (see Fig. 5). Data from panel 300-1 specimens are shown in Fig. 20 with solid lines, and data from panel 300-3 specimens are shown with dashed lines. Test data for nine of the ten coupons show a jump in strain around 3.5 kips. This jump is believed to correspond to failure of the gap filler material. Coupon CTE-300-3-HT-P-2 did not show this jump in strain, possibly due to the manufacturing nonconformity in this specimen in which the load introduction inserts are offset from each other by 0.25 in. (see Table 1). The non-zero value of strain at zero load for coupon CTE-300-3-HT-P-2 is possibly due to failure of the gap filler during installation in the load cell due to the offset of the specimen. The significant nonlinearity seen in the test results occurs after the gap filler fails and continues until the final failure load.

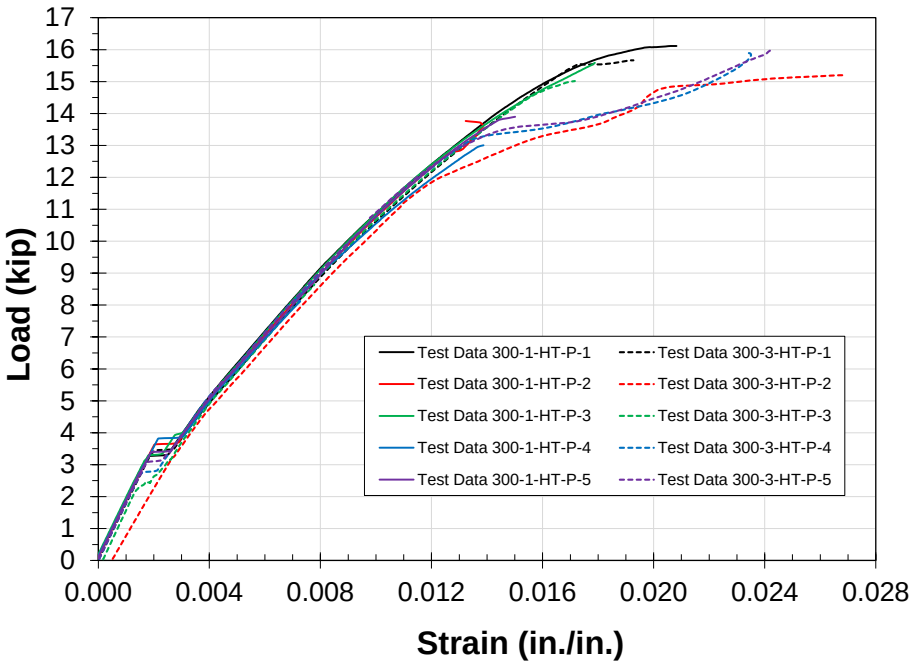

Figure 20: Load vs. strain test data for strain gage 1.

Fig. 21 contains test data from two representative specimens (300-1-HT-P-1 and 300-1-HT-P -2) and numerical data from Models 1 to 4. In Fig. 21, strain results for Models 1 to 4 are consistent with the test data until the assumed gap filler failure. Strain data from the nonlinear analysis of Model 3 follows the linear model responses until a load of 3.5 kips, after which the slope of the strain curve is reduced, due to plasticity of the gap filler. At a load of 13 kips, predicted strains in Model 3 from the linear and nonlinear analyses are 44% and 26 % lower than the test data, respectively. Strain results from Model 4 exhibit nonlinear behavior similar to the Model 3, although the explicit data is noisy compared to the implicit model. For Model 4, the predicted failure load and strain at failure are 15% and 39% lower than the test results, respectively, than for specimen CTE-300-1-HT-P-2. In addition to net section failure of the doubler plate and delamination, another possible cause of the nonlinearity in the test data is plasticity of the fabric doubler plate, as observed in Ref. 16. Unfortunately, a composite material model representing nonlinear behavior of the fabric was not available to the authors of this paper, and the numerical models do not represent this potential effect.

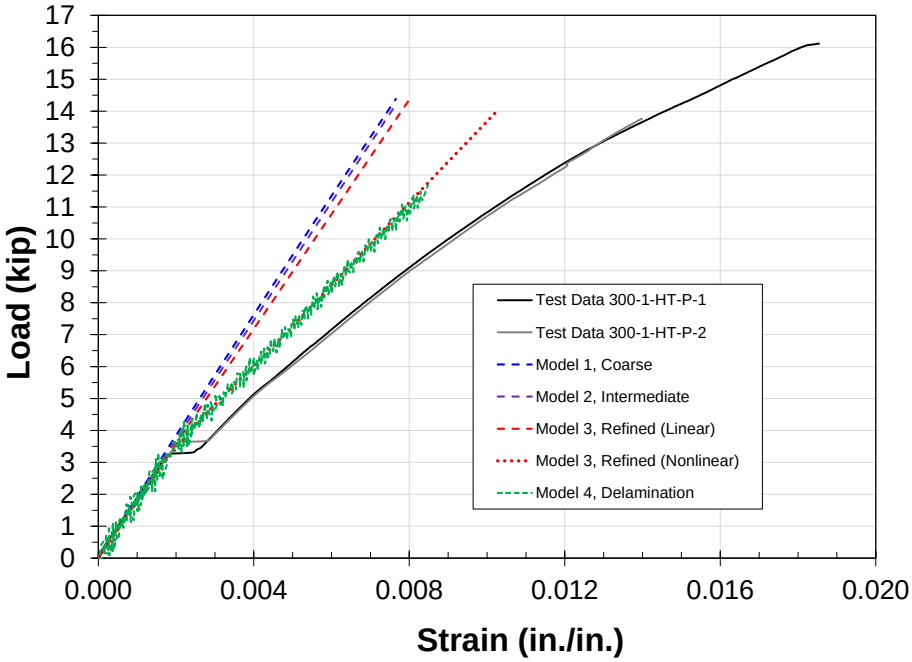

Figure 21. Load vs. strain test-analysis correlation for gage 1.

Strain contours from DIC of coupon CTE-300-1-HT-2 are presented in Fig. 22 along with predicted results from the nonlinear version of Model 3 and Model 4. In both the numerical models and the test data, the maximum tensile axial strain occurs in the middle of the coupon at the joint. The strain field is relatively uniform across the width of the specimen. Unfortunately the upper limit of the DIC color spectrum is below the maximum strain level in the test. In Fig. 22, far-field stress contours from Models 3 and 4 outside the region of the joint compare well with the DIC data. Strain results from Model 3 are below the values observed in the test due to nonlinearity of the test data (as shown in Fig. 21). Strain results from Model 4 are below the values observed in the test, but in Model 4 the analysis was stopped (due to delamination) at a load 15% below the load presented for the test data. As with the strain results presented in Fig. 20, it is believed that the fabric material in the doubler plates exhibits a nonlinear response that is not simulated in the numerical models. Because of the potential nonlinearity effect, the doubler plates in the test specimens were able to reach a higher strain level than could be predicted by the analysis methods presented in this paper, and further study of this effect is recommended.

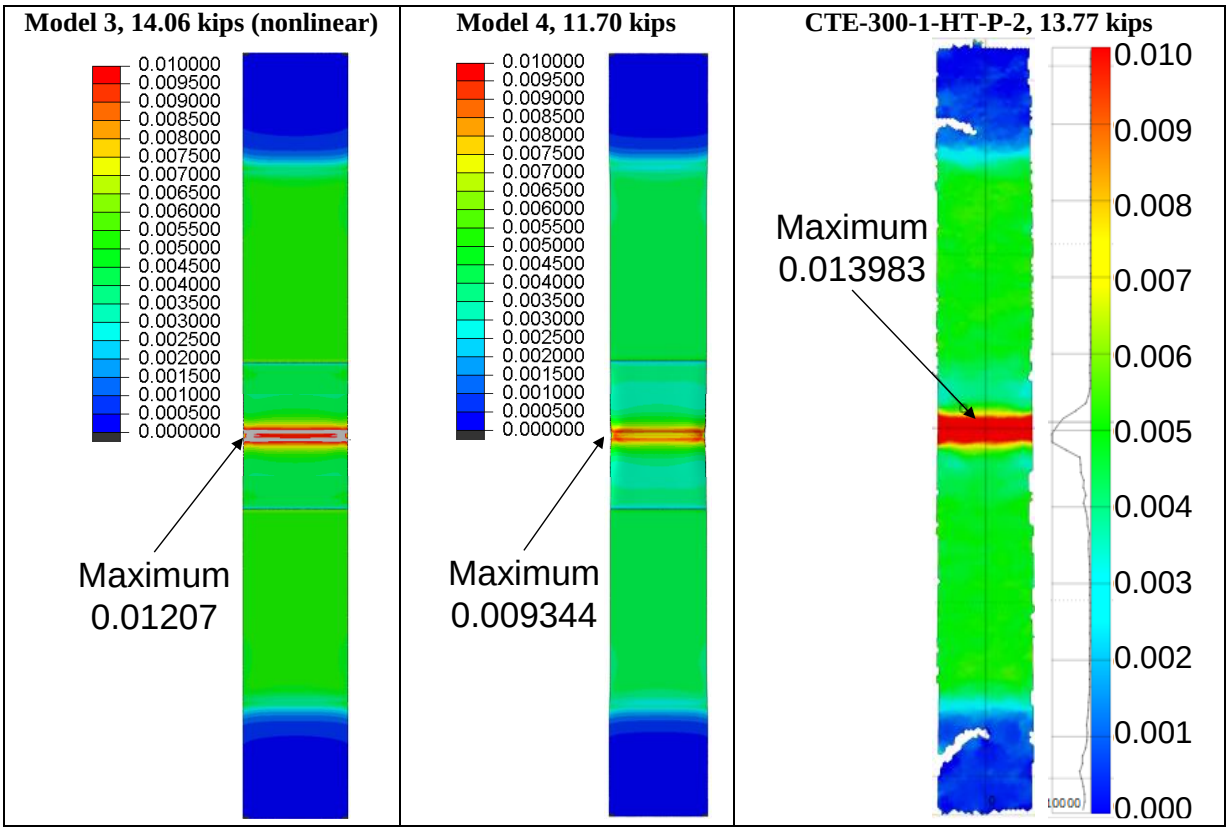

Figure 22. Strain contour plots for Model 3, Model 4, and test coupon CTE-300-1-HT-P-2 (units are in./in.).

V. Summary

A development effort of longitudinal joints for composite sandwich specimens is being conducted within the CTE project. One of the goals of this effort is to evaluate advanced analysis techniques, like cohesive zone modeling (CZM), virtual crack closure technique (VCCT), and progressive failure analysis (PFA), for use in predicting the structural failure of composite joints. Ten coupon specimens representing a longitudinal bonded composite joint were fabricated from larger panels and tested in July 2018. Results from the tests were compared with results from three finite element models: a coarse model, an intermediate model, a refined model, and a PFA model. Significant results of the test-analysis correlation are as follows:

1. Test coupons failed at an average load of 15.0 ksi, which is 5.56 times the design limit load.
2. Two main failure modes were observed in the test coupons: net-section failure of the doubler plates and delamination of the face sheets just below the face sheet/doubler-plate interface.
3. Test results for end displacement and far-field strain were mostly linear until specimen failure.
4. Test results for strains in the vicinity of the joint were linear until what was presumed to be a failure of the gap filler material around 3.5 kips.
5. Failure loads from the test were between 13 and 14 kips for specimens with delamination as the dominant failure mode. Failure loads from the test were between 15 and 16 kips for specimens with net-section failure (NSF) as the dominant failure mode. Three of the four specimens with a "mixed" failure mode fell within the NSF range; the other fell in the delamination range.
6. Based on load-displacement plots, the coarse and refined models matched the stiffness of the tested coupons (within 1%).
7. The predicted strain and displacement results for the linear coarse, intermediate, refined models were within 1%.
8. Using first ply failure theory, the nonlinear refined model underpredicted net section failure the of the test specimens by between 42% and 46%.
9. The refined nonlinear model captured some of the nonlinearity of the measured strain data from the test in the joint region, but the predicted strain response was 26% lower than the test data.

10. The predicted failure load from the delamination model was 10 to 15% lower than the failure load of the test coupons with delamination as a primary failure mode.
11. The delamination model captured the nonlinear strain response in the vicinity of the joint, but the predicted strain at failure was significantly lower (39%) than in the test.

Overall, all models matched the displacement and far-field strain data well; so, the geometry and elastic properties of the model are considered to be correct. The delamination model predicted the failure load within 10 to 15%, which is considered good, but could be improved with additional study. Final NSF of the doubler plate in the tests occurred at a much higher load than predicted by the Tsai Hill failure theory. It is noted that Tsai Hill is a first ply failure criterion that does not account for progression of damage in the model. Numerical results would likely be improved by further refinement of strength properties for the doubler plate, and by use of an analytical material model that represents shear nonlinearity and damage in a fabric composite.

VI. References

[1]Fikes, J. C., Jackson, J. R., Richardson, S. W., Thomas, A. S., Mann, T. O., and Miller, S. G., "Composites for Exploration Upper Stage," NASA/TM-2016-219433, December 2016.

[2]Mason, B. H., Sleight, D. W., and Grenoble R. W., "Test and Analysis Correlation for a Y-Joint Specimen for a Composite Tank," NASA/TM-2015-218967, October 2015.

[3]Johnson, T. F., Sleight, D. W., and Martin, R. A., "Structures and Design Phase I Summary for the NASA Composite Cryotank Technology Demonstration Project," AIAA Paper 2013-1825, 54th AIAA/ASME/ASCE/AHS/ ASC Structures, Structural Dynamics, and Materials Conference, Boston, MA, April 2013.

[4]Mann, T., Smeltzer, S., Grenoble, R. W., Mason, B. H., Rosario, S., and Fairbairn, R., "Sizing and Lifecycle Cost Analysis of an Ares V Composite Interstage," AIAA Paper 2012-1770, 53rd AIAA/ASME/ASCE/AHS/ASC Structures, Structural Dynamics, and Materials Conference, Honolulu, HI, April 2012.

[5]Turon, A., Dávila, C. G., Camanhi, P. P., and Costa, J., "An Engineering Solution for Mesh Size Effects in the Simulation of Delamination Using Cohesive Zone Models," *Engineering Fracture Mechanics*, Vol. 74, Issue 10, pp. 1665–1682, July 2007.

[6]Krueger, R., "Virtual Crack Closure Technique: History, Approach, and Applications," *Applied Mechanics Reviews*, Vol. 57, Issue 2, pp. 109–143, 26 April 2004.

[7]O'Brien, T. K., "Interlaminar Fracture Toughness: The Long and Winding Road to Standardization," *Composites, Part B: Engineering*, Vol. 29, Issue 1, pp. 57–62, 1998.

[8]O'Brien, T. K., "Characterization of Delamination Onset and Growth in a Composite Laminate," *Damage in Composite Materials*, ASTM STP 775, American Society for Testing and Materials, Philadelphia, PA, pp. 140–167, 1982.

[9]Satyanarayana, A., Bogert, P., Karayev, Z. K., Nordman, S. P., and Hamid, R., "Influence of Finite Element Size in Residual Strength Prediction of Composite Structures," AIAA Paper 2012-1619, 53rd AIAA/ASME/ASCE/AHS/ASC Structures, Structural Dynamics and Materials Conference, Honolulu, HI, April 2012.

[10]ABAQUS, *ABAQUS User's Manual*, Vol III, Version 6.12, Dassault Systèmes Simulia Corp., Pawtucket, RI, 2012.

[11]Jones, R. M., *Mechanics of Composite Materials, Second Edition*, Taylor and Francis, Philadelphia, PA, 1998.

[12]Dávila, C., Leone, A., Song, K., Ratcliffe, J., and Rose, C., "Material Characterization for the Analysis of Skin/Stiffener Separation", American Society of Conposites 32nd Technical Conference, Purdue University, West Lafayette, IN, October 23-25, 2017.

[13]Man, M., "Cytec Cycom 5320-1 T650 3k PW Fabric Qualification Material Property Data Report", National Institute for Aviation Research, NCAMP Test Report # CAM-RP-2012-017 Rev NC, October 13, 2015.

[14]http://www.aero-consultants.ch/view/data/3285/Produkte/Henkel Adhesive/ LOCTITE 9396 AERO.pdf.

[15]Hashin, Z., and Roten, A., "A Fatigue Failure Criterion for Fiber-Reinforced Composite Materials," *Journal of Composite Materials*, Vol. 7, October 1973, pp. 448-464.

[16]Cousigné, O., Moncayo, D., Coutellier, D., Camanho, P., and Naceur, H., "Numerical Modeling of Nonlinearity, Plasticity, and Damage, in CFRP-woven Composites for Crash Simulations," *Composite Structures*, Vol. 115, April 2014, pp. 75-88.